NANOSYSTEMS: PHYSICS, CHEMISTRY, MATHEMATICS, 2014, 5 (1), P. 178–185

FIELD ELECTRON EMISSION FROM A NICKEL-CARBON NANOCOMPOSITE

V. S. Protopopova, M. V. Mishin, A. V. Arkhipov, S. I. Krel, P. G. Gabdullin

Saint Petersburg State Polytechnic University, Saint Petersburg, Russia

max@mail.spbstu.ru, arkhipov@rphf.spbstu.ru

PACS 79.70.+q; 79.60.Jv; 81.05.uj; 81.07.-b

The field-emission properties of nanocomposite films comprised of 10 – 20 nm-sized nickel particles immersed in a carbon matrix were investigated. The films were deposited onto silicon substrates by means of a metal-organic chemical vapor deposition (MOCVD) method. The composite's structure was controlled via deposition process parameters. Experiments demonstrated that the composite films can efficiently emit electrons, yielding current densities of up to 1.5 mA/cm^2 in electric fields below 5 V/μm. Yet, good emission properties were only shown in films with low effective thickness, when nickel grains did not form a solid layer, but left a part of the substrate area exposed to the action of the electric field. This phenomenon can be naturally explained in terms of the two-barrier emission model.

Keywords: Amorphous carbon, Nanocomposite, Thin film, Field electron emission.

1. Introduction

Many different varieties of carbon-based nanostructures demonstrate the property of facilitated field-induced electron emission, even those having a relatively smooth surface without protruding fibers, sharp tips or ribs [1–16]. The role of their nano-scale structure in the emission mechanism may lie with their long-term confinement of hot electrons at high-energy states without thermalization, which creates favorable conditions for the subsequent transfer of those electrons into a vacuum, even in a moderate electric field [17]. These hot electrons may be generated when current flows through tunnel junctions separating emitter nanodomains. The discussed hypothesis [17] explains facilitated emission from heterogeneous carbon films comprised by both sp^2 (conductive) and sp^3 (weakly conductive) carbon phases. In the presented work, we investigated properties of nanocomposite films produced via the joint deposition of carbon and nickel on silicon substrates. The conductive phase in the deposited film was represented by Ni and/or graphitic carbon, while nickel carbide and/or sp^3-bonded carbon comprised a weakly conductive medium. Introduction of the second element provided additional flexibility to the technology, allowing manipulation of the composite structure via variation of the deposition process parameters.

In accordance with the two-barrier emission model [12–17], the size of the conductive crystallites can have dramatic effect on the emission properties of the film, while other parameters of this film's components are less important. Therefore the investigated Ni-C films could have been expected to demonstrate facilitated field electron emission with characteristics comparable to those of fully carbonic films of similar morphology [16].

2. Sample fabrication, structure and properties

The Ni-C thin films were prepared on Si substrates by the method of metal-organic chemical vapor deposition (MOCVD) with bis-(ethylcyclopentadienyl) nickel $(EtCp)_2Ni$ as the precursor. The deposition process was carried out in a hot-wall horizontal low-pressure tube

silica reactor with temperature maintained from 350 – 650 °C. Details of this technology may be found elsewhere [18].

The effective thickness of the deposited Ni layers was determined by means of X-ray fluorescence (XRF) spectroscopy (Spectroscan MAX-GV), via measurement of intensity of a Ni characteristic line. Morphology of deposited films was studied by scanning electron microscopy (SEM) (microscope Supra 55 VP).

The performed experiments demonstrated that composite film structure could be efficiently controlled via deposition process parameters: deposition time, substrate temperature and partial pressures of the precursor $(EtCp)_2Ni$, the H_2 and the buffer gas, Ar. In all cases, the film composition included carbon in an amorphous form. At the beginning of the deposition process, the Ni component was represented by separate nanoparticles occupying only a small part of the substrate surface. Then, the size and number of Ni particles increased until they merged into a solid film completely covering the substrate. Further deposition resulted in the formation of multi-layer films. The process affected not only the quantity of the precipitated metal but also the composite structure– both metallic particles and bonding carbon matrix. Fig. 1 presents a plot of surface electric resistivity for composite film samples versus deposition time (the latter was showed to be proportional to the effective Ni layer thickness). The data are given only for films with full area coverage. Surprisingly, the resistivity increases with film thickness. We explain this feature by two phenomena accompanying the deposition process. One of them involves the formation of carbide shells around Ni grains, which increases the insulating gaps separating adjacent crystallites and reduces the tunneling current between the grains. The percolation current flowing through grain contacts and conductive paths in the carbon matrix also decreases because of progressing graphitization of sp^3 carbon in the previously deposited film layers. The process results in increased film porosity (due to large difference in mass density between graphitic and the sp^3-bonded carbon forms, leading to the development of local mechanical strains and deformations during the phase transition), reduction of contact areas between Ni grains and the appearance of new inter-crystallite boundaries at current paths.

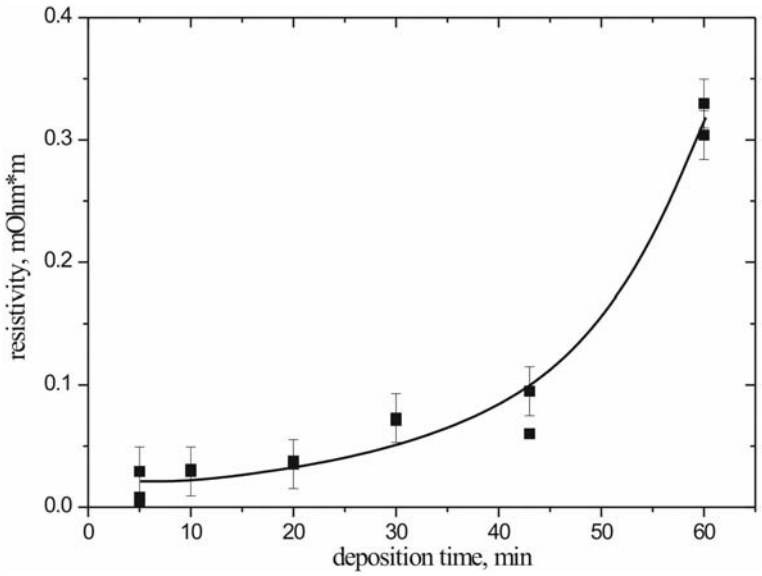

FIG. 1. Specific surface resistivity of Ni-C films deposited at 570 °C vs deposition time. Total pressure in reaction chamber 840 Pa, partial pressure of $(EtCp)_2Ni$ and hydrogen – 75 and 210 Pa respectively

TABLE 1. Sample surface morphology and deposition process parameters[1]

Sample	Temperature (°C)	Time (min)	Film morphology
1	390	60	Isolated particles, average size 11 nm
2	410	60	Isolated particles, average size 20 nm
3	570	5	Full monolayer of 20 nm particles, damaged during emission activation treatment
4	450	60	Full monolayer of 20 nm particles

[1]Total pressure in all cases was 840 Pa, partial pressure of $(EtCp)_2Ni$ and hydrogen – 75 and 210 Pa resp.

The substrate temperature maintained during the film fabrication process also had a strong effect on the resulting composite structure. The films deposited at higher temperatures were characterized by much greater porosity, lower density and higher surface resistivity. Also, substrate heating substantially increased the film growth rate.

For our emission experiments, we selected four samples with different film morphologies. The corresponding deposition process parameters and morphology types are listed in Table 1. Fig. 2 presents SEM images of the samples, showing mostly the Ni component of the composite. For the first two samples, the area density of Ni particles is low and they are isolated from each other. Hence, most of the weakly-conducting substrate's surface is open for penetration of external electric field. Mean particle size for samples 1 (Fig. 2(a)) and 2 (Fig. 2(b)) is equal to 11 nm and 20 nm, respectively. Samples 3 (Fig. 2(c)) and 4 (Fig. 2(d)) had full Ni grain monolayers completely covering the substrate. In the case of sample 3, the layer was deposited at a higher temperature (570 °C), and its mechanical strength was lower than that for sample 4, which was deposited in a much slower process at 450 °C. As a result, the former film was damaged in the course of emission activation treatment during the emission tests. (Fig. 2(c) shows its surface after the treatment). The film of sample 4 withstood the treatment without visible damage, as did samples 1 and 2, also deposited at low temperatures (390 °C and 410 °C respectively).

Besides Ni particles, the images of Fig. 2 show fiber-like structures that were identified as carbon nanocones [19], growing due to the high catalytic activity of Ni particles. According to [20] and references, the formation of silicon nanocones or combined Si/C structures is also possible under similar conditions (precursor pressure, Si substrate and its temperature). Though, efficient migration of silicon atoms through the silicon oxide layer and deposited film may be possible only in the presence of some activation factors. In [20], this role is ascribed to the flux of fast hydrogen ions generated in rf discharge and accelerated to the substrate by dc electric bias. In our case, the film deposition process did not engage application of either rf or dc field, hence we don't see any mechanisms for substrate atoms' mobility activation. In principle, the nanocones (either carbon or silicon) could substantially contribute to electron emission due to high local enhancement of applied electric field; hence their role in emission required a special investigation.

3. Emission tests

Field emission properties of the prepared Ni-C film samples were tested using the layout and experimental procedures described previously [21]. The electric field was applied in 0.5 – 0.6 mm-wide planar gap between the tested sample and tungsten cylindrical anode with ~ 30 mm^2 area. The tests were performed at a residual gas pressure of $\sim 10^{-7}$ Torr. Emission characteristics were measured with slowly increasing gap voltage $U(t)$ up to a maximum value

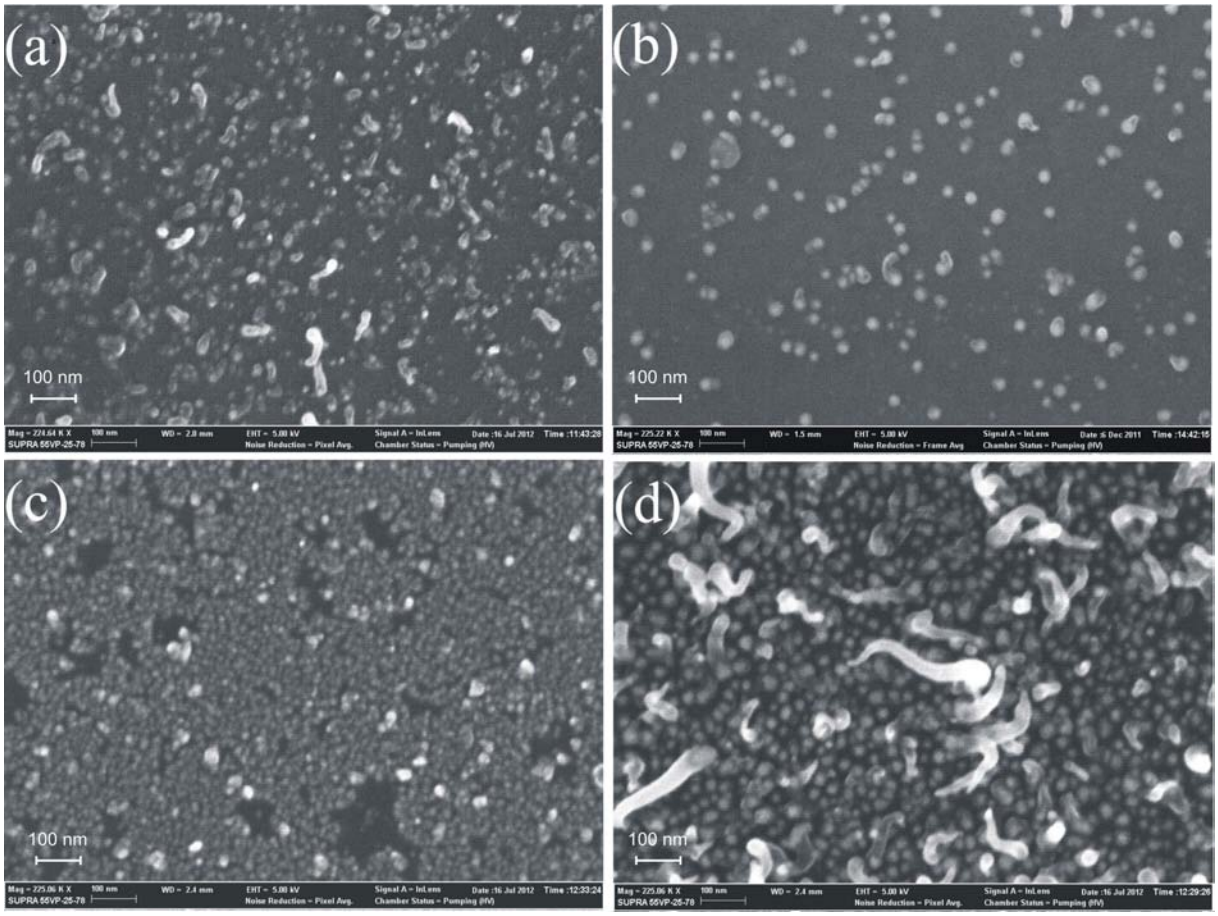

FIG. 2. SEM images of Ni-C films selected for the emission tests. (a) – sample 1; (b) – sample 2; (c) – sample 3 (after the tests); (d) – sample 4

$U_{\max}$. Then, the voltage was slowly decreased, and the 'reverse' branch of the characteristics was registered. The full cycle took approximately 65 seconds. This measurement was performed initially at room temperature and for relatively low $U_{\max}$. If no emission current appeared, the procedure was then repeated with greater $U_{\max}$ and/or higher sample temperature, until a measurable current was yielded. Then the sample was maintained under conditions where the emission current amounted to a few μA. In this situation, the sample's emission activity usually improved with time, and temperature and applied voltage were correspondingly decreased to stabilize the extracted current. After this activation treatment, the emission characteristics were measured repeatedly.

The performed experiments demonstrated that Ni-C film samples 1, 2 and 3 were capable of low-field electron emission. Their best emission characteristics are showed in Fig. 3. Emission started at threshold field values as low as 2 – 4 V/μm. Such values are very typical for numerous reported observations of low-field emission from various nanostructures, including different types of nanocarbon [1–17]. All characteristics were approximately linear in Fowler-Nordheim coordinates (bottom plot in Fig. 3), which gives evidence for the field-induced nature of the observed emission.

Figure 4 presents a typical temperature dependency of I–V emission plots for one of the samples. A temperature rise notably increased the emission current in comparison with its room-temperature value. Though, the dependency was relatively slow – sample heating to 380 °C resulted only in $\sim$ 100% current growth. In Fowler-Nordheim coordinates (bottom

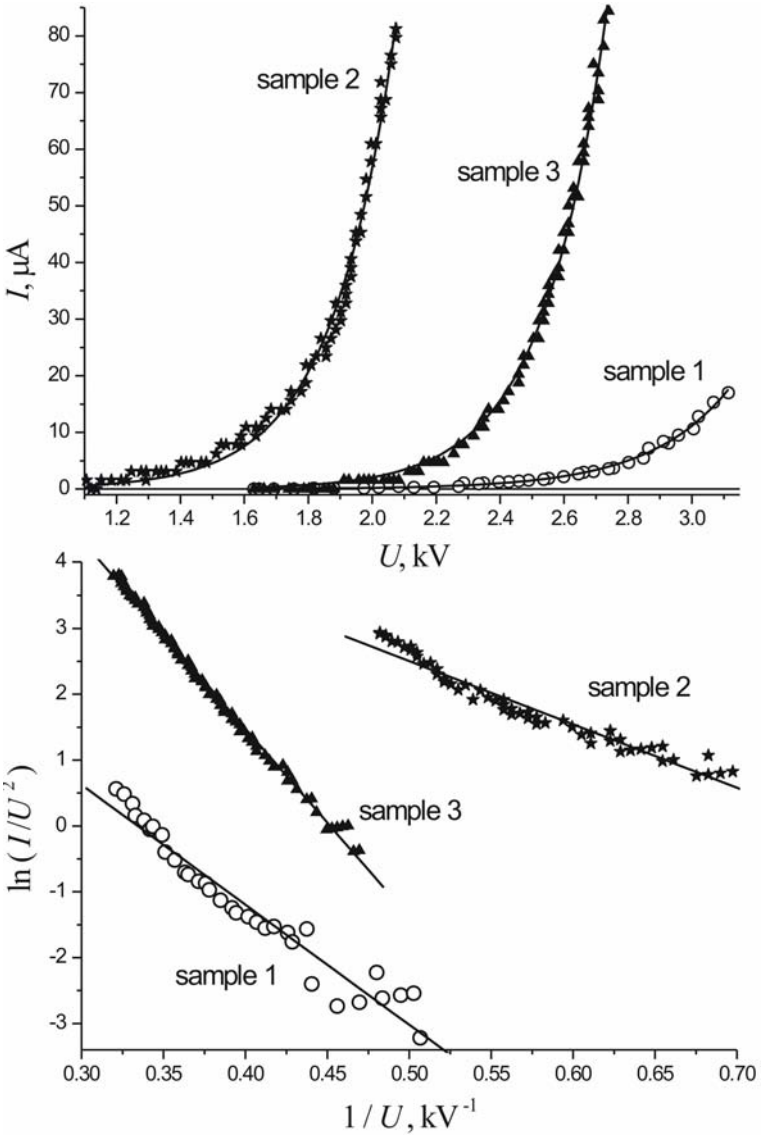

FIG. 3. Emission I–V plots of film samples measured in straight (top) and Fowler-Nordheim coordinates. The dependencies were measured at 380 °C

plot in Fig. 4) the linear emission plot was subject to approximately parallel displacement. The phenomenon of field emission thermal dependency is well known for different forms of nanocarbon [22–24]. It is usually explained by increased electron supply of emission sites due to substrate resistance reduction or increasing transparency of internal junctions, or by an increase of electron population of energy levels associated with surface, defects or dopant atom (that serve as intermediary states in emission mechanism), or by modification of emitter surface (due to out-gassing).

Sample 2 showed the best emission properties among the tested structures, with a threshold field value close to 2 V/μm. As it can be seen in Fig. 2, this film is comprised by separate 20 nm Ni particles. Previously, we observed [16] that purely graphitic carbon films of similar structure and dimensions also showed the best results. Sample 1, where the Ni grains were smaller ($\sim$ 11 nm), had an emission threshold that was twice as large. This observation is in good agreement with the estimates made in [17], demonstrating that the electric field induced

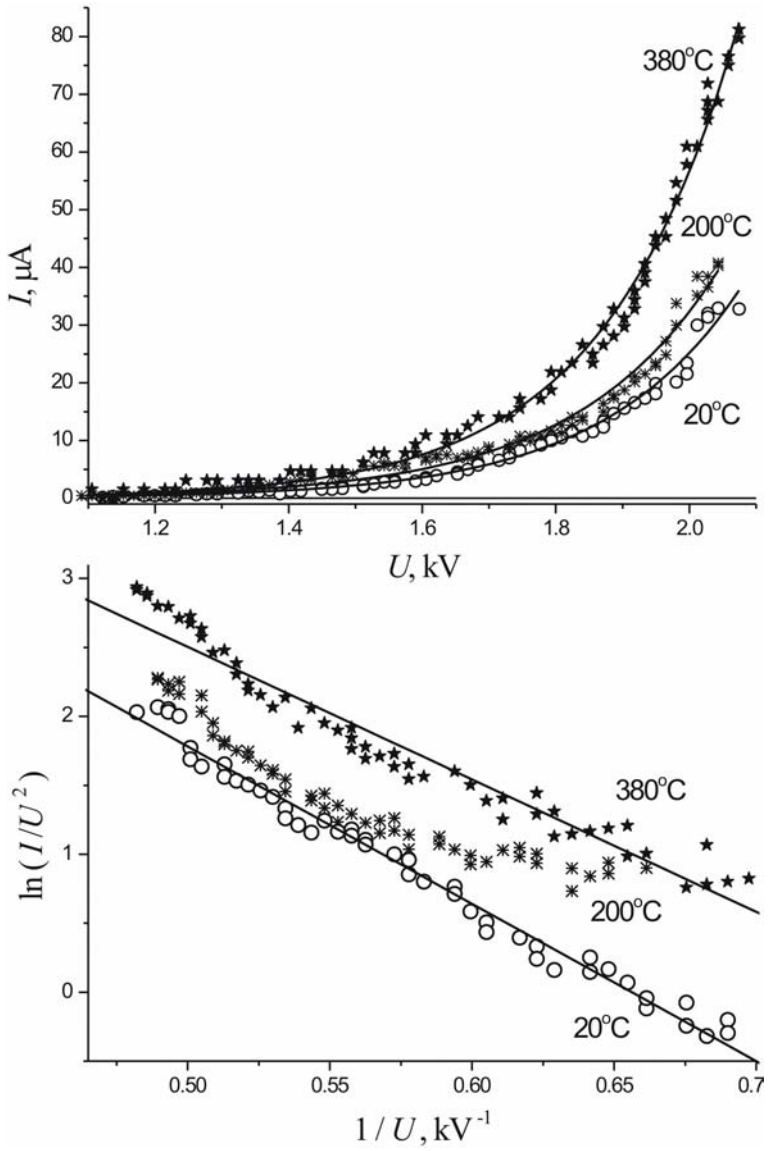

FIG. 4. Emission I–V plots of film sample 2 (see details in text and Table 1) measured at different temperatures

by an externally applied field between a substrate and an electrically insulated particle is proportional to particle size. Thus, the tunneling transport of electrons into a larger particle will produce hot electrons of a given energy (that can be responsible for facilitated emission) at lower value of the external field.

Emission from the sample 3 (that initially represented a solid film with 100% substrate coverage) appeared only after intensive activation treatment. We think that the activation which occurred was associated with the damage to the film caused by this procedure, opening a part of substrate surface (see in Fig. 2(c)) to the action of applied field. Its penetration under the film may have resulted in the generation of hot electrons. In contrast, sample 4 represented a film of similar morphology but with greater mechanical strength, that withstood the treatment undamaged. This sample never yielded any detectable emission current in the field up to $\sim$ 10 V/μm at temperatures up to 470 °C. Thus, we can associate emission with field penetration

in the sample. Surface conductivity of intact film (measured as approximately 10^4 S/m) is too high to allow substantial field penetration, which is necessary for generation of hot electrons.

The lack of emission for sample 4 also suggests that the nanocones (abundantly present at its surface, see Fig. 2d) did not play a key role in emission. This conclusion can be expanded onto the other samples, where concentration of the nanocones was much lower.

4. Summary

The experiments performed in the present work demonstrated that:

- Ni-C nanocomposite films can be fabricated by the MOCVD method from $(EtCp)_2Ni/H_2$ gas mixture. The composite has the general form of 10 – 20 nm Ni particles in carbonic matrix. Physical characteristics of the composite can be controlled via parameters of the film deposition process;
- the composite films at silicon substrates can serve as efficient cold electron emitters producing mean current densities in the mA/cm^2 range in electric field below 5 V/μm;
- electron emission was observed only for the films with relatively low effective thickness, with at least a part of the substrate surface open for the action of the applied field. This observation can be naturally explained in the hot-electron emission model.

Acknowledgments

The work was supported by the Russian ministry of education and science (grant No. 11.G34.31.0041) and by the RFBR (grant 13-02-92709).

References

[1] Okotrub A.V., Bulusheva L.G., et al. Field emission from products of nanodiamond annealing. *Carbon*, **42**, P. 1099–1102 (2004).
[2] Shpilman Z., Michaelson Sh., Kalish R., Hoffman A. Field emission measurements from carbon films of a predominant nano-crystalline diamond character grown by energetic species. *Diamond and Related Materials*, **15**, P. 846–849 (2006).
[3] Liu D., Benstetter G., Frammelsberger W. Nanoscale electron field emissions from the bare, hydrogenated, and graphitelike-layer-covered tetrahedral amorphous carbon films. *J. Appl. Phys.*, **99**, P. 044303 (2006).
[4] ZhaoY., Zhang B., et al. Improved field emission properties from metal-coated diamond films. *Diamond and Related Materials*, **16**, P. 650–653 (2007).
[5] Orlanducci S., Fiori A., et al. Nanocristalline diamond films grown in nitrogen rich atmosphere: structural and field emission properties. *J. Nanosci. Nanotechnol.*, **8**, P. 3228–3234 (2008).
[6] Panwar O.S., Rupesinghe N., Amaratunga G.A.J. Field emission from as grown and nitrogen incorporated tetrahedral amorphous carbon/silicon heterojunctions grown using a pulsed filtered cathodic vacuum arc technique. *J. Vac. Sci. Technol. B*, **26**, P. 566–575 (2008).
[7] Xu L., Wang C., et al. Effects of bonding structure from niobium carbide buffer layer on the field electric emission properties of a-C films. *J. Appl. Phys.*, **105**, P. 074318 (2009).
[8] Uppireddi K., Weiner B.R., Morell G. Field emission stability and properties of simultaneously grown micro-crystalline diamond and carbon nanostructure films. *J. Vac. Sci. Technol. B*, **28**, P. 1202–1205 (2010).
[9] Huang P.-C., Shih W.-C., Chen H.-C., Lin I-N. The induction of a graphite-like phase on diamond films by a Fe-coating/post-annealing process to improve their electron field emission properties. *J. Appl. Phys.*, **109**, P. 084309 (2011).
[10] Masuzawa T., Sato Y., et al. Correlation between low threshold emission and C–N bond in nitrogen-doped diamond films. *J. Vac. Sci. Technol. B*, **29**, P. 02B119 (2011).
[11] Nose K., Fujita R., Kamiko M., Mitsuda Y. Electron field emission from undoped polycrystalline diamond particles synthesized by microwave-plasma chemical vapor deposition. *J. Vac. Sci. Technol. B*, **30**, P. 011204 (2012).
[12] Karabutov A.V., Frolov V.D., et al. Low-field electron emission of diamond/pyrocarbon composites. *J. Vac. Sci. Technol. B*, **19**, P. 965–970 (2001).

[13] Obraztsov A.N., Zakhidov Al.A. Low-field electron emission from nano-carbons. *Diamond and Related Materials*, **13**, P. 1044–1049 (2004).
[14] Xie W.G., Chen Jun, et al. Effect of hydrogen treatment on the field emission of amorphous carbon film. *J. Appl. Phys.*, **101**, P. 084315 (2007).
[15] Filip L.D., Palumbo M., Carey J.D., Silva S.R.P. Two-step electron tunneling from confined electronic states in a nanoparticle. *Phys. Rev. B*, **79** (24), P. 245429 (2009).
[16] Arkhipov A.V., Gabdullin P.G., et al. Field-induced electron emission from graphitic nano-island films at silicon substrates. *Fullerenes, Nanotubes and Carbon Nanostructures*, **20** (4–7), P. 468–472 (2012).
[17] Arkhipov A.V., Gabdullin P.G., Mishin M.V. On possible structure of field-induced electron emission centers of nanoporous carbon. *Fullerenes, Nanotubes and Carbon Nanostructures*, **19** (1–2), P. 86–91 (2011).
[18] Alexandrov S.E., Protopopova V.S. Chemical vapor deposition of Ni-C films from bis-(ethylcyclopentadienyl) nickel. *Journal of Nanoscience and Nanotechnology*, **11**, P. 8259–8263 (2011).
[19] Baylor L.R., Merkulov V.I., et al. Field emission from isolated individual vertically aligned carbon nanocones. *J. Appl. Phys.*, **91** (7), P. 4602–4606 (2002).
[20] Orlanducci S., Toschi F., et al. A viable and scalable route for the homogrowth of Si nanocones and Si/C nanostructures. *Cryst. Growth Des.*, **12**, P. 4473–4478 (2012).
[21] Bondarenko V.B., Gabdullin P.G., et al. Emissivity of powders prepared from nanoporous carbon. *Tech. Phys.*, **49**, P. 1360–1363 (2004).
[22] Liao L., Zhang W.F., et al. Investigation of the temperature dependence of the field emission of ZnO nanorods. *Nanotechnology*, **18**, P. 225703 (2007).
[23] Tordjman M., Bolker A., Saguy C., Kalish R. Temperature dependence of reversible switch-memory in electron field emission from ultrananocrystalline diamond. *Appl. Phys. Lett.*, **101**, P. 173116 (2012).
[24] Arkhipov A.V., Gordeev S.K., et al. Nanodiamond composite as a material for cold electron emitters. *J. Phys.: Conf. Ser.*, **100**, P. 072047 (2008).